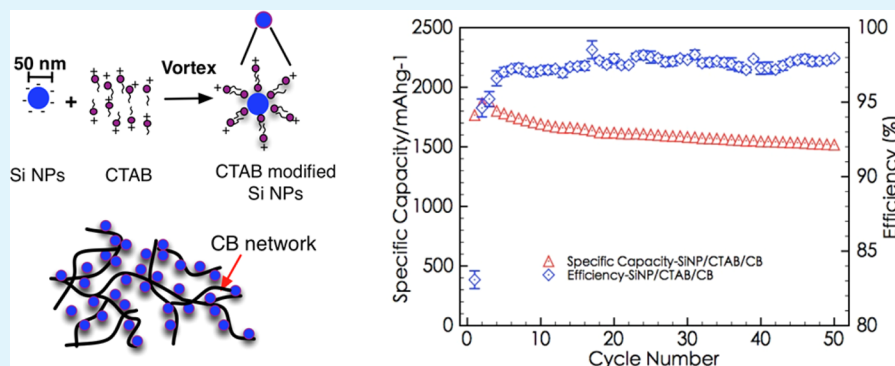# All-Aqueous Directed Assembly Strategy for Forming High-Capacity, Stable Silicon/Carbon Anodes for Lithium-Ion Batteries

Yanjing Chen,[†] Mengqing Xu,[‡] Yuzi Zhang,[†] Yue Pan,[‡] Brett L. Lucht,[‡] and Arijit Bose*,[†]

[†]Department of Chemical Engineering and [‡]Department of Chemistry, University of Rhode Island, Kingston, Rhode Island 02881, United States

ABSTRACT: Silicon (Si) particles have emerged as a promising active material for next-generation lithium-ion battery anodes. However, the large volume changes during lithiation/delithiation cycles result in fracture and pulverization of Si, leading to rapid fading of performance. Here, we report a simple, all-aqueous, directed assembly-based strategy to fabricate Si-based anodes that show capacity and capacity retention that are comparable or better than other more complex methods for forming anodes. We use a cationic surfactant, cetyltrimethylammonium bromide (CTAB), to stabilize Si nanoparticles (SiNPs) in water. This suspension is added to an aqueous suspension of para-amino benzoic acid-terminated carbon black (CB), pH 7. Charge interactions cause the well-dispersed SiNP to bind to the CB, allowing most of the SiNP to be available for lithiation and charge transfer. The CB forms a conducting network when the suspension pH is lowered. The dried SiNP/CTAB/CB anode exhibits a capacity of 1580 mAh g^{-1} and efficiency of 97.3% after 50 cycles at a rate of 0.1C, and stable performance at cycling rates up to 5C. The directed spatial organization of the SiNP and CB using straightforward colloidal principles allows good contact between the well-dispersed active material and the electrically conducting network. The pore space in the CB network accommodates volume changes in the SiNPs. When CTAB is not used, the SiNPs form aggregates in the suspension, and do not contact the CB effectively. Therefore, the electrochemical performance of the SiNP/CB anode is inferior to that of the SiNP/CTAB/CB anode. This aqueous-based, room temperature, directed assembly technique is a new, but simple, low-cost scalable method to fabricate stable Si-based anodes for lithium-ion batteries with performance characteristics that match those made by other more sophisticated techniques.

KEYWORDS: silicon−carbon anodes, all-aqueous processing, lithium ion batteries

■ INTRODUCTION

As the demand for future electric vehicles and portable electronics grows, advanced Li-ion batteries (LIB) will be required with long life, high power, and high energy density. Silicon (Si) has a theoretical specific capacity of 3580 mAh g^{-1} and is a promising material to replace graphite (capacity of 372 mAh g^{-1}), which is commonly used in anodes in current LIBs.[1−3] However, the large volume changes in silicon during lithiation and delithiation cycles result in its fracture and pulverization, and loss of contact of active material with the current collector, leading to rapid capacity fading. These volume changes also contribute to continuous mechanical degradation of the solid electrolyte interphase (SEI), exposing fresh Si to the electrolyte which results in continuous formation of the SEI. This contributes to capacity fading and poor Coulombic efficiency.[4−10]

Various approaches have been employed to overcome this problem, geared toward controlling the architecture and placement of the active material, Si, and the conductive carbon, in the anode. Different Si architectures include nanowires,[11,12] nanotubes,[13,14] nanoporous structures[15,16] and their composites with carbon black, graphite and graphene.[17,18] These anodes exhibit high capacity and good cycle stability. Fabrication of anodes using vapor phase growth processes is typically slow and costly, and is not ideal for scaling up to large volume

production. In this paper, we report a simple, inexpensive, aqueous-based colloidal processing strategy to form SiNP-carbon composite anodes. The key features of the anode are a uniform distribution of SiNP and good contact of these particles with a conducting carbon network. The SiNPs are stabilized by a charged surfactant, and these charged particles then bind to oppositely charged conducting carbon black particles that form the network. The pore spaces in the network accommodate volume changes in the SiNP during cycling. We demonstrate superior cycling performance of the anodes prepared using our strategy over anodes made without the surfactant. The performance of our anode compares very favorably with those made by other more complex methods.[8,12,13,19−25]

■ EXPERIMENTAL DETAILS

Preparation of SiNP/CTAB/CB and SiNP/CB Anodes. A para-amino benzoic acid-terminated carbon black (CB) suspension in water at pH 7.0 (Cabot Corporation) was used in this study. The CB particles have a specific surface area of ∼200m^2.g^{-1}. The pK_a of the acid is ∼6.5. Thus, the exposed carboxyl groups are deprotonated at pH 7.0. Si nanoparticles of average diameter 50 nm were purchased from Alfa Aesar. 50 mg of SiNPs were sonicated for 1 h in 1 mL of DI water, then 600 μL of a 5 mM CTAB aqueous solution was added into this SiNP suspension. The concentration and volume of the CTAB solution is about 10% higher than that required for complete bilayer coverage of all SiNP particles. After another 30 min of sonication, a 1.5%w/w CB suspension was added to produce a mass ratio of SiNP/CB of 2:1. This is followed by another 30 min of sonication. An aqueous solution of the binders carboxymethyl cellulose (CMC) and poly(acrylic acid) (PAA, MW ∼ 300,000) at a mass ratio of 1:1 was then added. The volume of the CMC/PAA solution is adjusted so that the final concentration of binder after drying is 25%w/w of the total anode mass (the SiNP, CB, and binder).[20,26] The sample was then placed in a vacuum oven at 50 °C and concentrated to a slurry. A doctor blade was used to coat the slurry onto Cu foil with thickness between 150−200 μm. The samples were then dried overnight at 120 °C under a vacuum. The area loading of the anode materials on the Cu foil was ∼0.35 mg/cm^2. The preparation technique is identical for the SiNP/CB anodes, except no CTAB is added.

Electrochemical Characterization. Individual 13 mm diameter circular electrodes were hole-punched from the coated Cu foil. CR2032 type coin cells were assembled in an argon-filled glovebox (oxygen <0.1 ppm, water <1 ppm) using Li foil as the counter electrode. Two separators, one Celgard 2325 and the other made from glass fiber, were used. The electrolyte was 1.0 M LiPF$_6$ in a mixture of ethylene carbonate (EC)/ ethylmethyl carbonate (EMC)/ fluoro-ethylene carbonate (FEC) in a 45:45:10 ratio by volume. The electrolyte components were obtained from BASF. We note that CTAB has essentially no solubility in this electrolyte, and thus should not affect the electrolyte even after multiple cycles.

The half cells were subjected to galvanostatic (constant current) lithiation/delithiation cycles from 0.05 to 1.5 V versus Li/Li$^+$ at 25 °C on an Arbin BT 2000 cycler. A current density of ∼30 μA cm^{-2} was used for experiments at 0.05C. The current densities were proportionally adjusted for the other lithiation/delithiation rates. For typical experiments, the first three cycles were conducted at 0.05C, to form the SEI layer. The remaining 47 cycles were conducted at 0.1C. The anode performance at faster rates, up to 5C, was also probed. All specific capacities were calculated based on the total mass of the SiNP, CB, and binder on the electrodes.[26−28]

Electrochemical Impedance Spectroscopy (EIS). EIS was performed on a Princeton Instruments V3 Potentiostat at 1 V after the cells were cycled at 25 °C at a charged state. The perturbation is 10 mV with a frequency range from 20 mHz to 1 × 10^5 Hz. The impedance was measured after 3 cycles at 0.05C and then after 50 cycles at 1C.

Analytical Characterization. *Transmission Electron Microscopy (TEM).* Fresh and cycled electrodes after 50 cycles were characterized using a JEOL 2100 transmission electron microscope. A small piece of the electrode was dispersed in dimethyl carbonate using sonication. This process broke the samples into small enough pieces for the internal structures to be observed at high magnification. A drop of the dispersion was then placed on a TEM grid and dried in a vacuum oven. The grid was stored in an argon-filled vial until it was observed. Samples were loaded rapidly into the TEM to minimize ambient exposure.

Cryogenic Transmission Electron Microscopy (Cryo-TEM). We used a novel, blotless and shear-free, cryo-TEM technique to provide an artifact-free image that shows the locations of the CB and SiNP in the suspension.[29] This is important, as typical cryo-TEM techniques use blotting to thin the sample on a grid, which also introduces high shear. Blotting can sometimes cause preferential absorption of particles, whereas shear can break particle networks. Thus, both blotting and shear can result in samples that are not representative of particle locations in the original suspension. We did not have binder in these samples, as that would prevent us from imaging the nanoparticles. We diluted the samples 500 times, and injected 3 μL on to the center of a holey carbon grid through a glass tube of inner diameter 344 μm. A capillary suction tube was placed at the edge of the grid, oriented parallel to the grid plane. This tube removed all the excess fluid on the grid and left thin films of the sample spanning the grid holes. The placement of the suction capillary implies essentially no flow in the grid holes during removal of excess liquid, thus eliminating any shear on the sample that was being observed. Subsequently, the grid bearing the sample was plunged into a liquid ethane reservoir, cooled by liquid nitrogen to a temperature close to its freezing point. The rapid vitrification of the sample preserved the particle locations as they were in the original suspension. The grid was then transferred on to a Gatan 626DH cold stage, and inserted into the TEM for imaging. The sample temperature was maintained at −165 °C at all times during imaging, and low-dose microscopy was used, to prevent the amorphous-to-crystalline phase transformation in vitrified ice or any beam-induced artifacts in the specimens. A slight underfocus was used to improve contrast.

Scanning Electron Microscopy (SEM). Small pieces of uncycled Si/CB and Si/CTAB/CB anodes were directly observed by SEM (Zeiss Sigma FE-SEM). For samples after cycling, the cells were disassembled in an argon-filled glovebox, harvested and rinsed with anhydrous dimethyl carbonate (DMC) three times to remove residual LiPF$_6$, followed by vacuum drying overnight at room temperature. The samples were then observed using SEM.

X-ray Photoelectron Spectroscopy (XPS). The cycled cells were disassembled in an argon glovebox, and the electrodes were harvested and rinsed with anhydrous dimethyl carbonate (DMC) 3 times to remove residual LiPF$_6$, followed by vacuum drying overnight at room temperature. Three coin cells were made for each type of electrode. A vacuum transfer vessel was used for air free analysis of the samples. XPS was performed on a Thermo Scientific K-Alpha system using Al Kα radiation (1486.6 eV) under ultrahigh vacuum conditions. The XPS peak positions were calibrated by recording spectra for the reference compounds LiF, PVDF, and Li$_x$PO$_y$F$_z$, which are present on the electrode surface. The graphite peak at 284.3 eV was used as a reference for the final adjustment of the energy scale in the spectra. The spectra were analyzed by Multipack 6.1A software. Line analyses of elemental spectra were conducted using Gaussian−Lorentzian (80:20) curve fitting. The cell to cell variability is less than 6%.

■ RESULTS AND DISCUSSION

Dissociation of surface silanol groups[30] produces a net negative charge on the SiNP when dispersed in water, producing a zeta potential of −1.8 mV. The repulsive interparticle interaction at this potential is not enough to prevent agglomeration of the SiNP due to attractive van der Waals forces between particles.[31] Addition of the cationic surfactant CTAB to the SiNP suspension results in bilayer adsorption on the particle surfaces,
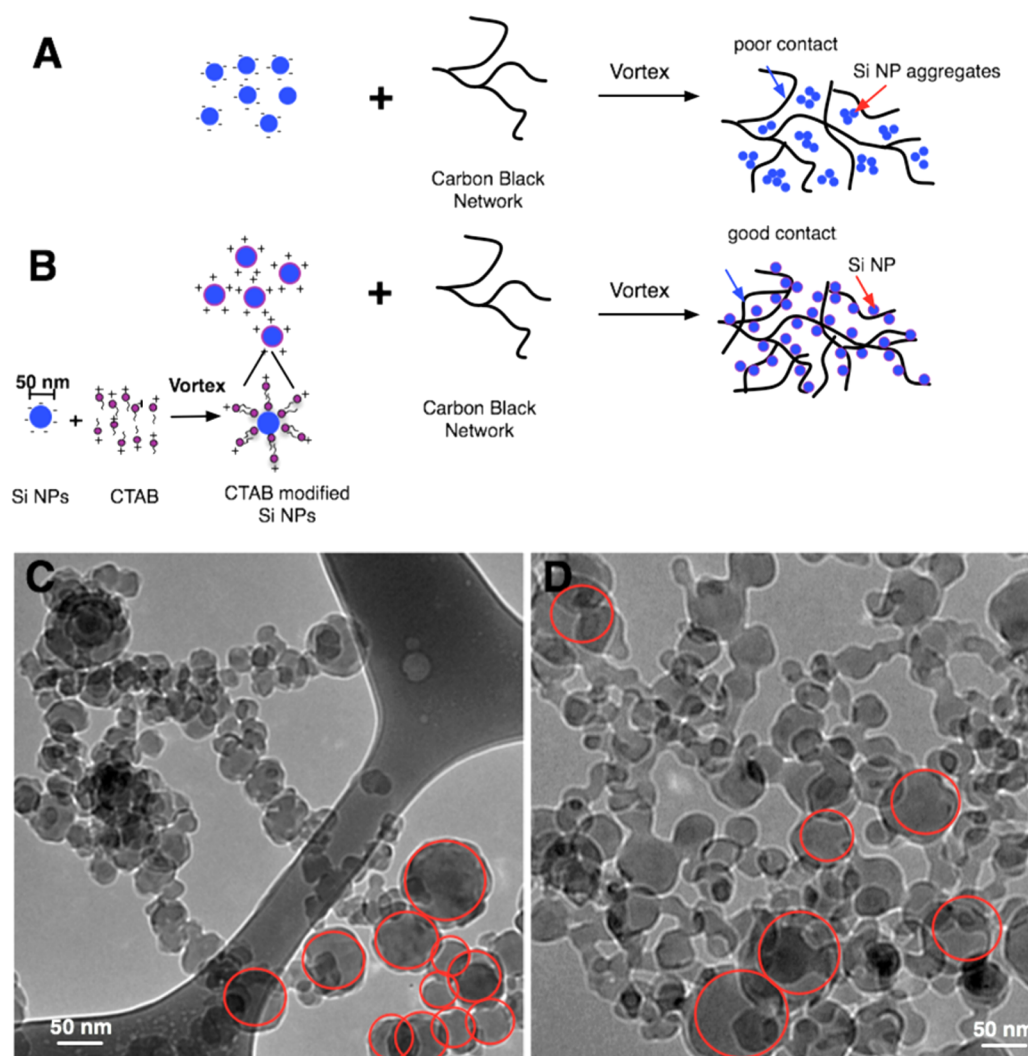
Figure 1. Illustration of Si/CB and Si/CTAB/CB anode preparation: (A) SiNPs are added directly to the CB suspension (B) SiNPs are exposed to CTAB in solution. The CTAB adsorbs as a bilayer on the surface of the particles, giving them a net positive charge. These positively charged particles bind to the negatively charged carbon black in the network. (C) Cryo-TEM image of the SiNP/CB suspension. The SiNPs are agglomerated. (D) Cryo-TEM image of the SiNP/CTAB/CB suspension. The SiNPs are well-distributed. The red circles in C and D indicate SiNPs.

and a zeta potential of +5.6 mV. This charge is adequate to stabilize the suspension.[31] The SiNP suspension is then added to a para-amino benzoic acid-terminated carbon black suspension in water. The pH of the suspension is lowered to 3, resulting in protonation of some surface carboxyl groups on the CB. The surface hydrophilicity of the CB particles decreases and they form a network in water.[32] Individual, positively charged SiNPs bind electrostatically to the negatively charged CB particles all along this network. As a control, the unmodified (no CTAB) SiNP suspension is added to the CB suspension. In this case, the charge on the particles and the charge on the CB surface are both negative, inhibiting SiNP attachment to the CB.[33] The anode formation strategies are shown in Figures 1A, B. In the remaining parts of this paper, the CTAB-containing sample is identified as SiNP/CTAB/CB, whereas the control is SiNP/CB.

Cryo-TEM images of the SiNP/CB and SiNP/CTAB/CB suspensions are shown in Figure 1C, D. The CB and SiNP were identified by their distinctive morphologies and by selected area energy-dispersive X-ray spectroscopy (EDX). The control sample shows agglomeration of the SiNP, whereas the SiNP/CTAB/CB sample shows the particles distributed more

uniformly. This difference has a strong impact on the performance of the anodes.

The electrochemical performance of the SiNP/CB and SiNP/CTAB/CB containing anodes for the first, fifth, 10th, 30th, and 50th cycles are shown in Figure 2.

The first reversible lithium charge capacities are 932 mAh.g^{-1} for the SiNP/CB and 1766 mAh g^{-1} for SiNP/CTAB/CB anodes, respectively. The capacity is calculated based on the total mass of SiNP, CB, and binder. The better dispersion of the SiNPs compared to the control case is responsible for the difference in performance. The fifth and later cycles display a higher capacity than in the first 4 cycles because Li ions are lost to SEI formation. Some of the capacity increase may also be due to electrode wetting and increased contact of the active material with the electrolyte during the initial cycling.

The maximum specific capacities were 1880 mAh g^{-1} for the third cycle and 1268 mAh g^{-1} for the fourth cycle of the SiNP/CTAB/CB and SiNP/CB anodes, respectively. The increase of specific capacity during the first few cycles is due to decreasing irreversible loss of Li ions once the SEI is formed.[34] At greater than 50 cycles, the SiNP/CTAB/CB anode exhibits a higher
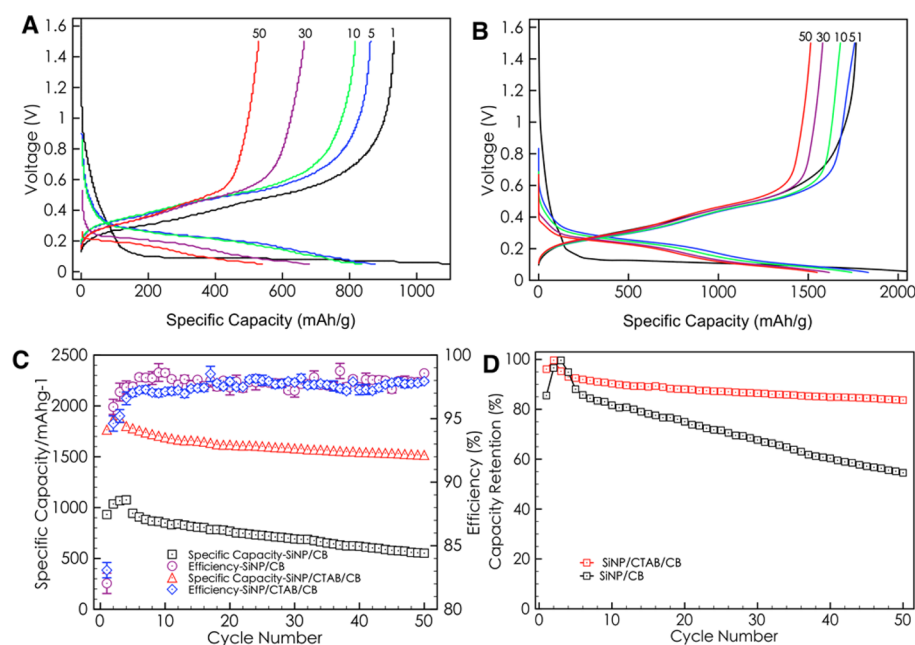
Figure 2. (A) Voltage versus Li/Li+ over the range 0.05−1.5 V for the SiNP/CB and (B) SiNP/CTAB/CB anodes, at charge/discharge rates of 0.1*C*. (C) Delithiation capacity and Coulombic efficiency of SiNP/CB and SiNP/CTAB/CB anodes at charge/discharge rates of 0.1*C*. For these experiments, the first three cycles were run at a rate of 0.05C to enable SEI formation. Two different anodes were prepared for both SiNP/CB and SiNP/CTAB/CB and the plots show the average from those samples. The error bars indicate the maximum spread in the data. (D) Comparison of the delithiation capacity retention for the SiNP/CB and SiNP/CTAB/CB anodes. The data are normalized by their respective maximum capacities.

delithiation capacity and a more stable cycle performance than the SiNP/CB anode.

Figure 2D shows the capacity retention, normalized by the maximum capacity. After 50 cycles, the SiNP/CTAB/CB anode fades to 84% of the maximum, whereas the SiNP/CB anode capacity decreases to 53% of its maximum value. A maximum capacity of 1788 mAh g^{-1} (the capacity is normalized by the weight of Si+CB+binder) and retention of more than 80% of the maximum capacity at the end of 50 cycles is a strong performance for a silicon-based anode.[35−37] The minimally aggregated SiNP allows most of the active material to be exposed and a stable SEI to form within the first few cycles. The good contact between SiNPs and CB network reduces contact resistance compared to the SiNP/CB sample. The unaggregated SiNPs also have room for expansion in the porous carbon black network, thus buffering any stresses that might cause them to fracture and reduce contact with the electrode.

We compared the performance of the SiNP/CTAB/CB and the Si/CB anodes at different cycling rates, and show the capacities in Figure 3. The SiNP/CTAB/CB anode maintains a high specific capacity at high rates, while the SiNP/CB anode has very little capacity at 5C. To examine if the changes to the anode were reversible, a lithiation/delithiation rate of 0.1*C* was applied following the 5C cycling rate. The specific capacity of SiNP/CTAB/CB anode recovered to 1552 mAh g^{-1}, which is 92% of the maximum. The anode with SiNP/CB was only 672 mAh g^{-1}, or 55% of the maximum. These results indicate that after rapid cycling, the SiNP/CTAB/CB anode architecture is essentially retained, while the SiNPs in the SiNP/CB anode might be getting pulverized. We note that most of the SiNP fracturing and pulverization happens in the first 10 cycles, as the capacity for both samples recovers to that value even after fast cycling.

Electrochemical impedance spectroscopy was conducted to further understand the performance of the anodes. For these
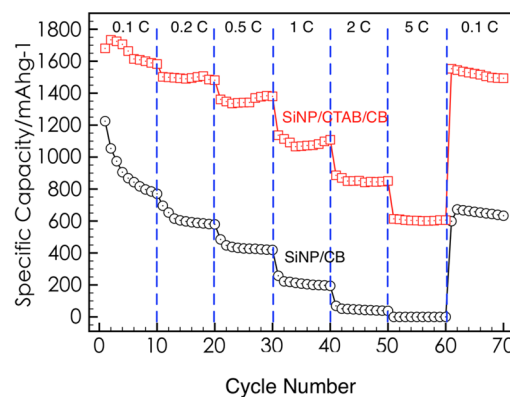

Figure 3. Capacities of SiNP/CTAB/CB (red) and SiNP/CB anodes at various charge rates ranging from 0.1*C* to 5*C*. A rate of 0.1*C* was applied at the end of process to test for reversibility.

measurements, each sample had 3 cycles at 0.05*C* followed by 50 cycles at 1*C*, and the results are shown in Figure 4. The SiNP/CTAB/CB sample has a much smaller SEI resistance R_f and charge transfer resistance R_{ct} compared to the SiNP/CB sample. The improved contact beween the SiNP and the conducting CB network for the SiNP/CTAB/CB sample produces lower impedance than in the SiNP/CB sample, and contributes to the improved cycling and rate performance of the former cell.

The morphology of anodes before and after cycling was observed by TEM. As shown in Figure 5A, C, the edges of SiNPs were observable in both fresh anodes. After 50 cycles, with the first 3 cycles at 0.05C, and the remaining cycles at 0.1*C*, SiNPs in SiNP/CB anode suffered significant pulverization and appeared porous (Figure 5B). For the SiNP/CTAB/CB anode, the spherical shape of SiNPs was retained and their edges remained clearly visible, as seen in Figure 5D. These
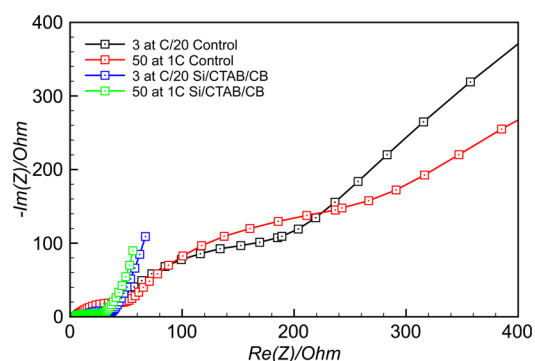
Figure 4. Electrochemical impedance spectra of SiNP/CB and SiNP/CTAB/CB after 3 cycles at 0.05C and 50 cycles at 1C.
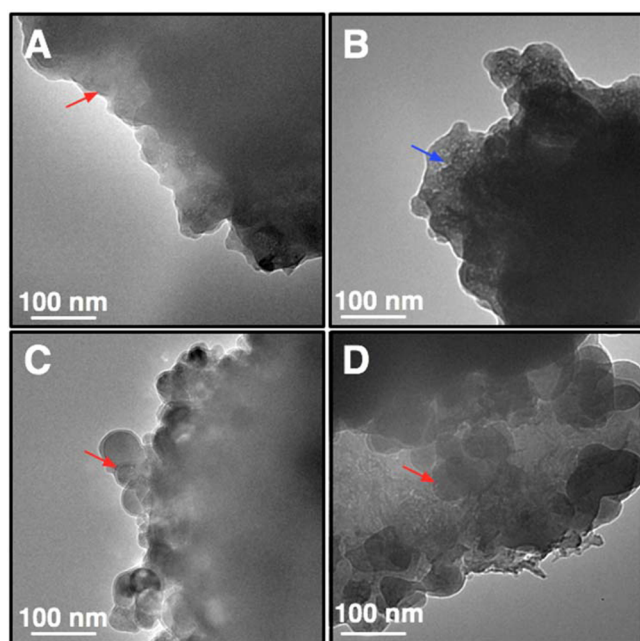

Figure 5. TEM images of (A) fresh SiNP/CB anode. (B) SiNP/CB anode after 50 cycles. (C) Fresh SiNP/CTAB/CB anode. (D) SiNP/CTAB/CB anode after 50 cycles. Blue arrow indicates the porous Si powder and the red ones indicate the edge of a SiNP.

results also indicate that the structural features of SiNP/CTAB/CB anode significantly reduce SiNP fracturing and pulverization. We confirm this observation by examining the anodes using SEM, before and after cycling (Figure 6). The surface of the SiNP/CB anode shows a rougher texture, indicative of pulverization (Figures 6A, B), whereas the surface of the SiNP/CTAB/CB anode appears only marginally degraded after cycling (Figure 6C, D).

To better understand the changes to the surface and structure of the SiNP/CB and the SiNP/CTAB/CB anodes, we acquired XPS spectra, which are shown in Figure 7. Fresh SiNP/CB and SiNP/CTAB/CB anodes have very silimar spectra (Figure 7A, B). After cycling, new species produced by electrolyte decomposition on the anode surface were observed (Figure 7C, D), supporting the formation of an SEI layer. However, significant differences were observed between the spectra from the SiNP/CTAB/CB and the SiNP/CB anodes. A higher concentration of CO_3^{2-} (Li_2CO_3 and lithium alkyl carbonates) was found on the SiNP/CTAB/CB anode surface, while a higher concentration of C=O (~288 eV) containing
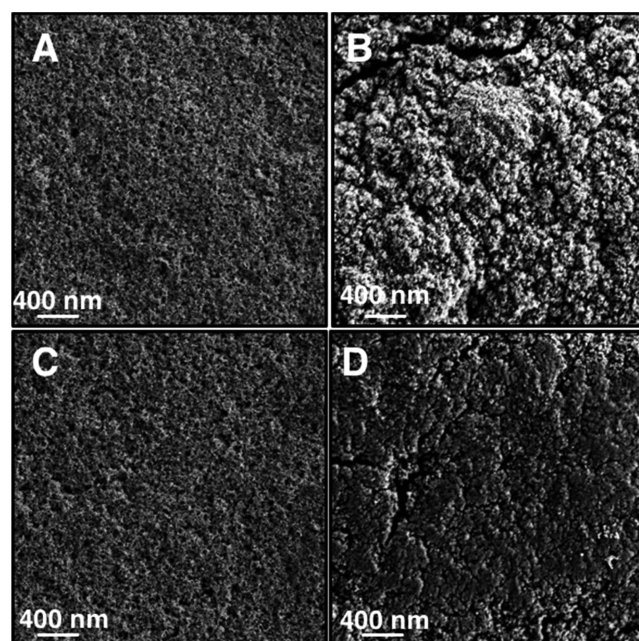

Figure 6. SEM images of the Si/CB anode (A) before and (B) after cycling. SEM images of the Si/CTAB/CB anode (C) before and (D) after cycling.

species was present on the surface of the SiNP/CB sample. In addition, the surface of SiNP/CB electrode has a higher concentration of LiF (22.5% F) compared to that of the SiNP/CTAB/CB (14.1% F) anode. The poor conductivity of LiF contributes to higher impedance and lower electrochemical performance. The lower concentration of LiF on the SiNP/CTAB/CB electrodes is consistent with an inhibition of electrolyte decomposition. This is a result of less SiNP pulverization on this anode, leading to a smaller increase in the surface area exposed to the electrolyte. Although we cannot confirm this, the CTAB can also be forming a protective coating on the SiNPs reducing their exposure to electrolyte (but does not significantly inhibit transport of Li ions).

We note here that the electrochemical performance SiNP/CTAB/CB anode is comparable to Si−C anodes made by a range of other techniques.[8,12,13,19,21−25,37−40] The key advantage of our method is the ease of processing and fabrication, which implies greater potential for scaling up at reduced processing costs.

■ CONCLUSIONS

We demostrate a simple aqueous-based strategy to fabricate Si anodes for lithium-ion batteries. SiNPs were uniformly dispersed in water containing a cationic surfactant CTAB, then added to a suspension of carboxyl-terminated CB in water. The SiNPs bind to the oppositely charged CB particles in the suspension. Because the SiNPs were uniformly dispersed, they were all available for lithiation and delithiation, providing high specific capacity. Capacity fade during fast charge and discharge rates was low. The excellent contact between SiNPs and CB increased the conductivity of anode. The pore spaces in the CB network permitted volume expansion and contraction of the SiNP without transmitting stresses to the conducting CB network. This room-temperature, all-aqueous strategy for forming stable, high-performance Si-based anodes is low-cost
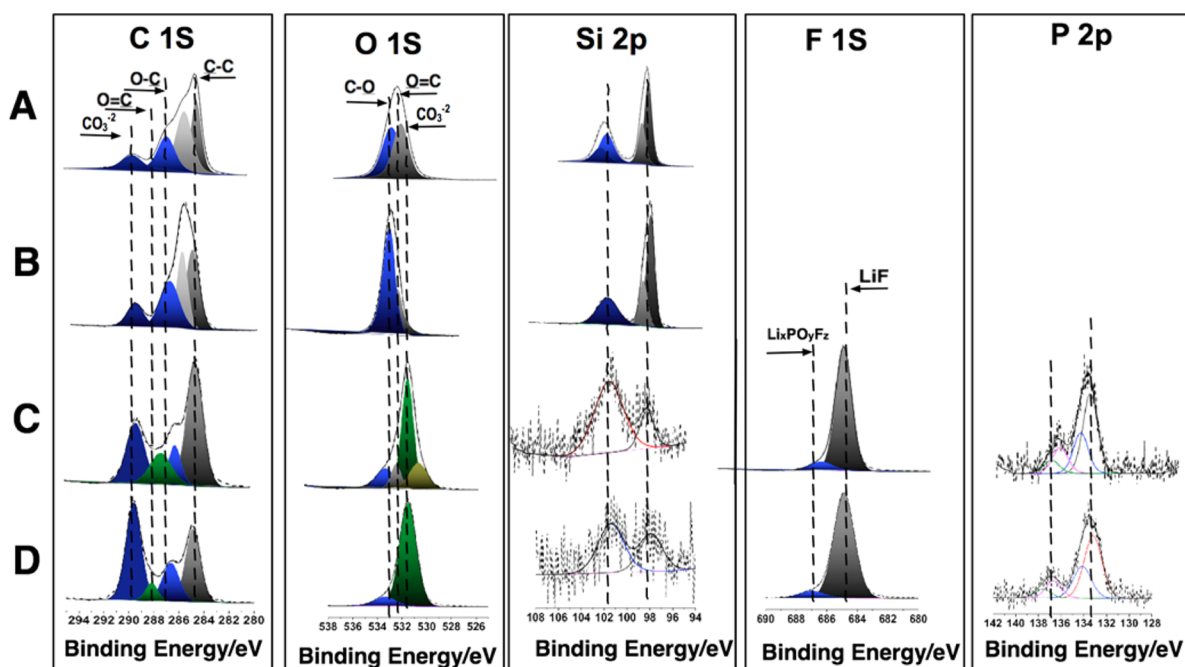
Figure 7. C 1s, O 1s, F 1s, Si 2p, and P 2p XPS spectra of the (A) fresh SiNP/CB anode, (B) fresh SiNP/CTAB/CB anode, (C) SiNP/CB anode after 50 cycles, and (D) SiNP/CTAB/CB anode after 50 cycles in 1.0 M LiPF$_6$ EC/DEC/FEC (45:45:10, vol %).

and potentially easily scalable. This is the main advantage of the fabrication technique.

■ AUTHOR INFORMATION

Corresponding Author
*E-mail: bosea@uri.edu. Phone: 401-874-2804.

Notes
The authors declare no competing financial interest.

■ REFERENCES

(1) Obrovac, M. N.; Christensen, L. Structural Changes in Silicon Anodes During Lithium Insertion/Extraction. *Electrochem. Solid-State Lett.* **2004**, *7*, A93–A96.

(2) Li, J.; Dahn, J. R. An in Situ X-Ray Diffraction Study of the Reaction of Li with Crystalline Si. *J. Electrochem. Soc.* **2007**, *154*, A156–A161.

(3) Shi, H.; Barker, J.; Saidi, M. Y.; Koksbang, R.; Morris, L. Graphite Structure and Lithium Intercalation. *J. Power Sources* **1997**, *68* (2), 291–295.

(4) Tarascon, J. M.; Armand, M. Issues and Challenges Facing Rechargeable Lithium Batteries. *Nature* **2001**, *414* (6861), 359–367.

(5) Hatchard, T. D.; Dahn, J. R. In Situ Xrd and Electrochemical Study of the Reaction of Lithium with Amorphous Silicon. *J. Electrochem. Soc.* **2004**, *151* (6), A838–A842.

(6) Xie, J.; Yang, X. G.; Zhou, S.; Wang, D. W. Comparing One- and Two-Dimensional Heteronanostructures as Silicon-Based Lithium Ion Battery Anode Materials. *ACS Nano* **2011**, *5* (11), 9225–9231.

(7) Key, B.; Bhattacharyya, R.; Morcrette, M.; Seznec, V.; Tarascon, J. M.; Grey, C. P. Real-Time Nmr Investigations of Structural Changes in Silicon Electrodes for Lithium-Ion Batteries. *J. Am. Chem. Soc.* **2009**, *131* (26), 9239–9249.

(8) Wu, H.; Zheng, G. Y.; Liu, N. A.; Carney, T. J.; Yang, Y.; Cui, Y. Engineering Empty Space between Si Nanoparticles for Lithium-Ion Battery Anodes. *Nano Lett.* **2012**, *12* (2), 904–909.

(9) Sethuraman, V. A.; Chon, M. J.; Shimshak, M.; Srinivasan, V.; Guduru, P. R. In Situ Measurements of Stress Evolution in Silicon Thin Films During Electrochemical Lithiation and Delithiation. *J. Power Sources* **2010**, *195* (15), 5062–5066.

(10) Nadimpalli, S. P. V.; Sethuraman, V. A.; Dalavi, S.; Lucht, B. L.; Chon, M. J.; Shenoy, V. B.; Guduru, P. R. Quantifying Capacity Loss Due to Solid-Electrolyte-Interphase Layer Formation on Silicon Negative Electrodes in Lithium-Ion Batteries. *J. Power Sources* **2012**, *215*, 145–151.

(11) Lin, L. H.; Sun, X. Z.; Tao, R.; Li, Z. C.; Feng, J. Y.; Zhang, Z. J. Photoluminescence Origins of the Porous Silicon Nanowire Arrays. *J. Appl. Phys.* **2011**, *110* (7), 073109.

(12) Cui, L.; Yang, Y.; Hsu, C.; Cui, Y. Carbon–Silicon Core–Shell Nanowires as High Capacity Electrode for Lithium Ion Batteries. *Nano Lett.* **2009**, *9* (9), 3370–3374.

(13) Cui, L. F.; Hu, L. B.; Choi, J. W.; Cui, Y. Light-Weight Free-Standing Carbon Nanotube-Silicon Films for Anodes of Lithium Ion Batteries. *ACS Nano* **2010**, *4* (7), 3671–3678.

(14) Park, M.-H.; Kim, M. G.; Joo, J.; Kim, K.; Kim, J.; Ahn, S.; Cui, Y.; Cho, J. Silicon Nanotube Battery Anodes. *Nano Lett.* **2009**, *9* (11), 3844–3847.

(15) Yu, Y.; Gu, L.; Zhu, C. B.; Tsukimoto, S.; van Aken, P. A.; Maier, J. Reversible Storage of Lithium in Silver-Coated Three-Dimensional Macroporous Silicon. *Adv. Mater.* **2010**, *22*, 2247–2250.

(16) Kim, H.; Han, B.; Choo, J.; Cho, J. Three-Dimensional Porous Silicon Particles for Use in High-Performance Lithium Secondary Batteries. *Angew. Chem., Int. Ed.* **2008**, *47*, 10151–10154.

(17) Jeong, S.; Lee, J.; Ko, M.; Kim, G.; Park, S.; Cho, J. Etched Graphite with Internally Grown Si Nanowires from Pores as an Anode for High Density Li-Ion Batteries. *Nano Lett.* **2013**, *13*, 3403–340.

(18) Bogart, D. T.; Oka, D.; Lu, X.; Gu, M.; Wang, C.; Korgel, B. A. Lithium Ion Battery Peformance of Silicon Nanowires with Carbon Skin. *ACS Nano* **2014**, *8* (1), 915–922.

(19) Cui, L.; Ruffo, R.; Chan, C. K.; Peng, H.; Cui, Y. Crystalline-Amorphous Core–Shell Silicon Nanowires for High Capacity and High Current Battery Electrodes. *Nano Lett.* **2009**, *9* (1), 491–495.

(20) Guo, Z. P.; Jia, D. Z.; Yuan, L.; Liu, H. K. Optimizing Synthesis of Silicon/Disordered Carbon Composites for Use as Anode Materials in Lithium-Ion Batteries. *J. Power Sources* **2006**, *159* (1), 332−335.

(21) He, Y. S.; Gao, P. F.; Chen, J.; Yang, X. W.; Liao, X. Z.; Yang, J.; Ma, Z. F. A Novel Bath Lily-Like Graphene Sheet-Wrapped Nano-Si Composite as a High Performance Anode Material for Li-Ion Batteries. *RSC Adv.* **2011**, *1* (6), 958−960.

(22) Hong, Li; Huang, X.; Chen, L.; Wu, Z.; Liang, Y. A High Capacity Nano-Si Composite Anode Material for Lithium Rechargeable Batteries. *Electrochem. Solid-State Lett.* **1999**, *2*, 547−549.

(23) Kong, J. H.; Yee, W. A.; Wei, Y. F.; Yang, L. P.; Ang, J. M.; Phua, S. L.; Wong, S. Y.; Zhou, R.; Dong, Y. L.; Li, X.; Lu, X. H. Silicon Nanoparticles Encapsulated in Hollow Graphitized Carbon Nanofibers for Lithium Ion Battery Anodes. *Nanoscale* **2013**, *5* (7), 2967−2973.

(24) Holzapfel, M.; Buqa, H.; Krumeich, F.; Novak, P.; Petrat, F.; Veit, C. Chemical Vapor Deposited Silicon/Graphite Compound Material as Negative Electrode for Lithium-Ion Batteries. *Electrochem. Solid-State Lett.* **2005**, *8* (10), A516−A520.

(25) Ng, S. H.; Wang, J.; Wexler, D.; Konstantinov, K.; Guo, Z. P.; Liu, H. K. Highly Reversible Lithium Storage in Spheroidal Carbon-Coated Silicon Nanocomposites as Anodes for Lithium-Ion Batteries. *Angew. Chem., Int. Ed.* **2006**, *45* (41), 6896−6899.

(26) Magasinski, A.; Zdyrko, B.; Kovalenko, I.; Hertzberg, B.; Burtovyy, R.; Huebner, C. F.; Fuller, T. F.; Luzinov, I.; Yushin, G. Toward Efficient Binders for Li-Ion Battery Si-Based Anodes: Polyacrylic Acid. *ACS Appl. Mater. Interfaces* **2010**, *2* (11), 3004−3010.

(27) Ko, M.; Chae, S.; Jeong, S.; Oh, P.; Cho, J. Elastic a-Silicon Nanoparticle Backboned Graphene Hybrid as a Self-Compacting Anode for High-Rate Lithium Ion Batteries. *ACS Nano* **2014**, *8* (6), 8591−8599.

(28) Chen, Y.; Nie, M.; Lucht, B. L.; Saha, A.; Guduru, P. R.; Bose, A. High Capacity, Stable Silicon/Carbon Anodes for Lithium-Ion Batteries Prepared Using Emulsion-Templated Directed Assembly. *ACS Appl. Mater. Interfaces* **2014**, *6* (7), 4678−4683.

(29) Lee, J.; Saha, A.; Pancera, S. M.; Kempter, A.; Rieger, J.; Bose, A.; Tripathi, A. Shear Free and Blotless Cryo-Tem Imaging: A New Method for Probing Early Evolution of Nanostructures. *Langmuir* **2012**, *28* (9), 4043−6.

(30) Behrens, H.; Grier, D. The Charge of Glass and Silica Surfaces. *J. Chem. Phys.* **2001**, *115*, 6716−6721.

(31) Israelachvili, J. *Intermolecular and Surface Forces*, 3rd. ed.;. Academic Press: London, 2011.

(32) Saha, A.; Nikova, A.; Venkataraman, P.; John, V. T.; Bose, A. Oil Emulsification Using Surface-Tunable Carbon Black Particles. *ACS Appl. Mater. Interfaces* **2013**, *5*, 3094−3100.

(33) Bi, Z.; Liao, W. Wettability Changes by Ctab Adsorption at Surfaces of Sio2 Film or Silica Gel Powder and Mimic Oil Recovery. *Acta Phys. Chim. Sin.* **2002**, *18* (11), 962−966.

(34) Nie, M.; Abraham, D. P.; Chen, Y.; Bose, A.; Lucht, B. L. Silicon Solid Electrolyte Interphase (Sei) of Lithium Ion Battery Characterized by Microscopy and Spectroscopy. *J. Phys. Chem. C* **2013**, *117* (26), 13403−13412.

(35) Ko, M.; Chae, S.; Jeong, S.; Oh, P.; Cho, J. Elastic Silicon Nanoparticle Backboned Graphene Hybrid as a Self-Compacting Anode for High-Rate Lithium Ion Batteries. *ACS Nano* **2014**, *8* (8), 8591−8599.

(36) Chang, J.; Huang, X.; Zhou, G.; Cui, S.; Hallac, P. B.; Jiang, J.; Hurley, P. T.; Chen, J. Multilayered Si Nanoparticle/Reduced Graphene Oxide Hybrid as a High-Performance Lithium-Ion Battery Anode. *Adv. Mater.* **2014**, *26*, 758−764.

(37) Lee, J. K.; Smith, K. B.; Hayner, C. M.; Kung, H. H. Silicon Nanoparticles−Graphene Paper Composites for Li Ion Battery Anodes. *Chem. Commun.* **2010**, *46*, 2025−2017.

(38) Choi, N. S.; Yew, K. H.; Choi, W. U.; Kim, S. S. Enhanced Electrochemical Properties of a Si-Based Anode Using an Electrochemically Active Polyamide Imide Binder. *J. Power Sources* **2008**, *177* (2), 590−594.

(39) Kasavajjula, U.; Wang, C. S.; Appleby, A. J. Nano- and Bulk-Silicon-Based Insertion Anodes for Lithium-Ion Secondary Cells. *J. Power Sources* **2007**, *163* (2), 1003−1039.

(40) Yoshio, M.; Wang, H.; Fukuda, K.; Umeno, T.; Dimov, N.; Ogumi, Z. Carbon-Coated Si as a Lithium-Ion Battery Anode Material. *J. Electrochem. Soc.* **2002**, *149* (12), A1598−A1603.